

Nature of Antenna Radiation Revealed by Physical Circuit Model

Yuhang Dou¹, Member, IEEE, and Ke-Li Wu², Fellow, IEEE

Abstract—Radiation efficiency of electrically small antennas largely depends on antenna geometry. However, the actual mechanism that governs the antenna radiation efficiency remains unclear, although various models have been developed since the 1940s. Extant circuit models are either intuition-based or mathematic representations of input impedance/far-field spherical mode functions for structurally simple antennas with limited uses and physical insight. In this article, a recently developed physical micromodeling circuit (MMC) model is utilized to explain the nature of radiation of an electrically small antenna of arbitrary configuration. It is theoretically discovered and experimentally validated for the first time that the radiation efficiency decisively depends on mutual radiated power associated with partial segments of the antenna. A circuitual figure of merit for describing the total mutual radiated power is introduced to quantify the measure. The graphical representation of the figure of merit called the holographic radiation diagram is also proposed for illustrating the correspondence of the positive and negative radiated power and the antenna structure. The applications of the proposed theory to antenna design is demonstrated by designing a highly efficient loop antenna. The physical circuit model paves a new way of understanding electromagnetic (EM) radiation problems.

Index Terms—Antenna, antenna couplings, circuit model, radiation efficiency.

I. INTRODUCTION

SINCE Guglielmo Marconi employed antennas and sent the first-ever wireless communication over the Bristol Channel with the message “Are you ready” on May 13, 1897 [1], the antenna has become an indispensable tool in the daily lives of human beings for transmitting and receiving signals through radio waves. Since then, efforts to elucidate the fundamental principles of antennas have never been ceased. Among these works, finding a physically sensible circuit model of an antenna that could represent the essence of the radiation of antennas has long constituted a challenge as a circuit model is the most familiar tool for electrical engineers. A physical circuit model of an antenna should not only facilitate antenna design specifically but also provide a

new perspective to understand the fundamental mechanisms of antennas in general.

However, such a physical circuit model was not easy to come by with conventional methods prior to knowing the current and charge distributions [2]. In the antenna community, the well-known Chu’s [3] theory is the most influential work, which estimates the lower bound of radiation quality factor Q and bandwidth for electrically small antennas. The theory defines an equivalent circuit using the recurrence formula of the spherical harmonics of electromagnetic (EM) waves for a structure unspecified small antenna. The approach that expands the far-field, the current on antenna surface, or the input impedance into spherical harmonics [4] is still found useful in recent works to estimate dissipation factors [5], to establish fundamental limits on the radiation efficiency of resonant electrically small antennas [6], and to find the maximum efficiency for some elementary shaped antennas [7]. An estimated bound by the modal expansion method, however, only provides a qualitative trend, rather than a design guideline for a given practical antenna configuration. The circuit models used are in a fixed circuit configuration to represent the input impedance in terms of harmonic functions. More references for the recent research on antenna radiation efficiency using modal analysis can be found in [6] and [7].

For optimum radiation efficiency, the optimal currents for canonical antennas were investigated using a numerical optimization method in recent years [8]. An equivalent high-order circuit model is used for antennas in a wide frequency range, which is obtained by fitting a high-order transformer circuit using a genetic algorithm [9]. An intuition-based circuit model is proposed to understand the coupling effect of a mobile terminal antenna [10]. An antenna circuit model fitted by input impedance provides a tool to integrate microwave structures into a time-domain simulation framework of a digital communication system [11]. However, the above-mentioned circuit models are either irrelevant to the antenna structure or are in a simple RLC circuit with an empiric parasitic capacitance, effective capacitance and inductance, and effective radiation resistance in a series combination [12]. By all means, a physical antenna circuit model would be more useful than a mathematic representation substitute. Toward this direction, a few structural-dependent circuit models were developed empirically for some simple commonly used antenna configurations, such as dipole and patch antennas [13]–[15].

A rigorous modeling of radiation problems using the partial element equivalent circuit (PEEC) model [16] is proposed

Manuscript received July 9, 2019; revised May 9, 2020; accepted June 20, 2020. Date of publication July 16, 2020; date of current version January 5, 2021. This work was supported by the University Grants Committee of Hong Kong under Grant AoE/P-04/08. (Corresponding author: Ke-Li Wu.)

Yuhang Dou was with the Department of Electronic Engineering, The Chinese University of Hong Kong, Hong Kong. She is now with the School of Electrical and Computer Engineering, Purdue University, West Lafayette, IN 47907 USA (e-mail: yuhang.dou@gmail.com).

Ke-Li Wu is with the Department of Electronic Engineering, The Chinese University of Hong Kong, Hong Kong (e-mail: klwu@cuhk.edu.hk).

Color versions of one or more of the figures in this article are available online at <https://ieeexplore.ieee.org>.

Digital Object Identifier 10.1109/TAP.2020.3008676

0018-926X © 2020 IEEE. Personal use is permitted, but republication/redistribution requires IEEE permission.

See <https://www.ieee.org/publications/rights/index.html> for more information.

for free-space problems in [17], in which the capacitance is delicately treated as purely real whereas its radiation resistance embedded in complex partial inductance equals to that of a Hertzian dipole. This work spurs investigation of distributive radiation and transferred power with the PEEC model with complex partial capacitance and inductance by complying with the energy conservation law globally [18], [19]. The investigation looks at the aggregated power of the radiated and the reactively transferred between two antennas. Due to the nonphysical nature, the PEEC model with complex partial capacitance and inductance could not interpret the radiated power from partial segments of an antenna.

Recently, the characteristic modes (CMs) theory [20]–[22] has regained tremendous attention as a facilitator for antenna designs. The applications of the theory also include estimation of radiation efficiency of characteristic currents [23].

To a certain extent, the existing work on antenna radiation efficiency could not reveal the physical nature of antenna radiation due to lacking an accurate description of the interaction of partial antenna segments and a legitimate explanation of how the radiation is related to the interaction. It seems that more attention is paid to the aggregated radiated power but little effort on how the radiated power is built up. The limitations of existing circuit models refrain people from a deeper understanding of the nature of antenna radiation because the models are not physical. As will be shown in this article, the essential characteristics of an antenna depend decisively on the interaction of partial segments of the antenna structure, i.e., partial mutual couplings and the phases of relevant currents in the circuit domain language. Correct information about mutual couplings, which includes electric mutual coupling (mutual capacitance), magnetic mutual coupling (mutual inductance), and mutual radiation resistance, must be incorporated in a legitimate circuit model. Such exquisitely fine information would be difficult to obtain without a rigorous, systematic, and mathematic process.

To investigate the nature of antenna radiation, the full-wave micromodeling circuit (MMC), which is developed recently for packaging and interconnection problems [24], [25], is employed for the antenna problem. The circuit is derived directly and systematically from Maxwell's equations. The MMC provides a new view of antenna radiation problems from a sensible and holistic circuit domain perspective. In addition to traditional antenna characteristics, such as input impedance and CMs, most significantly, the MMC model renders a holographic radiation diagram that can explain how the positive and negative radiated power is associated with the mutual couplings of partial antenna segments. It is discovered, for the first time, that it is the radiated power from mutual radiation resistance that decisively determines the radiation efficiency, rather than self-radiation resistance. Unlike the existing theory for estimating a bound for the radiation efficiency, it will be shown that the full-wave circuit model can not only provide an accurate calculation of but also guide to improve the radiation efficiency. As a side product, the MMC model can also be used to compute CMs very efficiently. With the aid of the proposed circuitual figure of merit and the holographic radiation diagram, one can identify the “ghost” CM, whose

negative radiated power is comparable to the positive radiated power.

This article contains three parts: first, the generality of the MMC circuit is briefly reviewed. Then, the description of antenna radiation problems from the full-wave MMC circuit perspective is presented followed by an introduction to formulating a CM equation using the MMC circuit. Three example antennas with different working modes are used to demonstrate the effectiveness of the MMC to antenna problems and how to use the theory to understand the mechanism of antenna radiation. An illustrative example is given to show how to use the holographic radiation diagram to improve a loop antenna design by enhancing the radiation efficiency from 66% to 99% theoretically, or from 57% to 91% experimentally.

In addition to presenting the MMC theory to the antenna designers specifically, and to investigating the EM radiation problem in general, the main contributions of this work are threefold: 1) proposing a new circuitual figure of merit to describe the radiation efficiency, which provides a new perspective for understanding antennas; 2) discovering the fact that the radiation efficiency is decisively determined by the radiated power from the mutual radiation resistance; and 3) depicting the partial radiated power by means of a holographic radiation diagram of the working current and a characteristic current mode for a given antenna configuration and providing a unique tool for antenna designers.

II. MICROMODELING CIRCUIT

The MMC is a full-wave circuit model derived from the generalized partial element equivalent circuit (G-PEEC) model, which is based on the mixed potential integral equation (MPIE) for multiple conductors, an integral form of Maxwell's equations [17]. The derivation of an MMC constitutes two processes: formation of a mesh-dependent circuit model from the discretized MPIE with excessive partial circuit elements, and a physically meaningful node-absorbing process applied to the circuit. The latter absorbs the insignificant nodes one by one until the broad sense and narrow sense stopping criteria are satisfied.

A. Circuit Interpretation of MPIE

The circuit model, which is known as the G-PEEC [17], is developed from the full-wave MPIE

$$\frac{\mathbf{J}(\mathbf{r})}{\sigma} = -\nabla \int_S \frac{1}{\varepsilon_0} G(\mathbf{r}, \mathbf{r}') \rho(\mathbf{r}') ds' - j\omega \int_S \mu_0 G(\mathbf{r}, \mathbf{r}') \cdot \mathbf{J}(\mathbf{r}') ds' \quad (1)$$

where ρ and \mathbf{J} are the surface charge and surface current densities on conductor surfaces, respectively. For a free-space multiple conductor problem, without losing generality, G is the full-wave scalar potential Green's function in free space. To obtain the G-PEEC model, the surface charge and current densities in (1) are discretized by the capacitive and inductive meshes [16], as shown in Fig. 1. By applying the Galerkin's matching procedure on each inductive mesh of the discretized form of (1) and conflating the nonstatic portion in the first

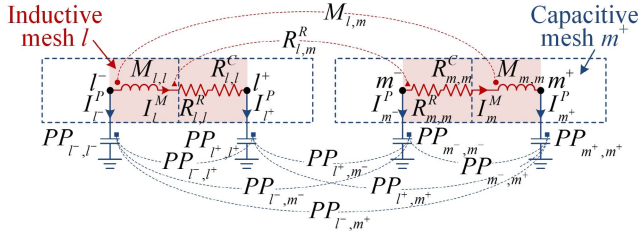


Fig. 1. Mesh and circuit interpretation of MPIE. Subscripts l and m refer to the indices of inductive meshes. Subscripts l^+ , l^- , m^+ , and m^- refer to the indices of capacitive meshes.

term on its right-hand side into the second term, (1) becomes the Kirchhoff's voltage law (KVL) equation, whose circuit representation is embedded in Fig. 1

$$R_l^C I_l^M + \sum_m R_{l,m}^R I_m^M + \sum_m j\omega M_{l,m} I_m^M + \sum_n \frac{1}{j\omega} [PP_{l^+,n} - PP_{l^-,n}] I_n^P = 0 \quad (2)$$

where

$$R_l^C = l_l / \sigma a_l \quad (3)$$

$$R_{l,m}^R = \text{Re}[j\omega M_{l,m}''] \quad (4)$$

$$M_{l,m} = \text{Re}[M_{l,m}''] \quad (5)$$

$$PP_{l^\pm,n} = \frac{1}{\varepsilon_0 S_{l^\pm} S_n} \int_{S_{l^\pm}} \int_{S_n} G_0(\mathbf{r}, \mathbf{r}') ds' ds \quad (6)$$

and subscripts l and m refer to the indices of inductive meshes. The two end capacitive meshes for inductive meshes l and m are notated by subscripts l^+ , l^- , m^+ , and m^- , respectively. Subscript n refers to the general index of a capacitive mesh, which is the placeholder of subscripts l^+ , l^- , m^+ , and m^- . σ and ε_0 are conductivity and permittivity in free space. In (6), G_0 is the static part of the Green's function; I_l^M is the conductive current on inductive mesh l flowing from node l^- to node l^+ ; and I_n^P is the displacement current flowing from node n to the ground, which corresponds to the derivative of the charge on capacitive mesh n with respect to time. Resistance R_l^C reflects the conductor loss on inductive mesh l . $R_{l,m}^R$ and $R_{l,m}^R$ are the self-radiation resistance of inductive mesh l and mutual radiation resistance between inductive meshes l and m . $M_{l,l}$ and $M_{l,m}$ are the self-inductance of inductive mesh l and inductive coupling between inductive meshes l and m , respectively. $PP_{n,n}$ is the coefficient of potential with respect to the capacitive mesh n . $PP_{l^\pm,n}$ represents the capacitive coupling between capacitive meshes l^\pm and n . As analogous to capacitance of a capacitor, the self-term $PP_{n,n}$ is called self-potance of potior n , and the mutual term $PP_{l^\pm,n}$ is called mutual potance between potiors l^\pm and n in the context. To simplify the illustration, a branch that contains a serial inductor, a loss resistor, and a radiation resistor, hereinafter, is denoted as a composite inductor M'' that is expressed by

$$M_{l,m}'' = \frac{\mu_0}{w_l w_m} \int_{S_l} \int_{S_m} (\mathbf{t}_l \cdot \mathbf{t}_m) G(\mathbf{r}, \mathbf{r}') ds' ds + [M'_{l^-,m^+} - M'_{l^-,m^-} - M'_{l^+,m^+} + M'_{l^+,m^-}] \quad (7)$$

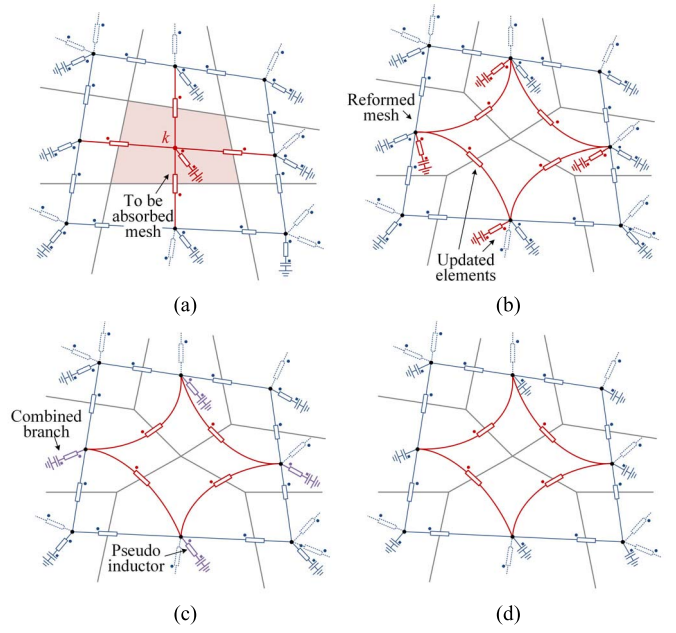


Fig. 2. Node-absorbing process. (a) Circuit with a node k to be absorbed. (b) Intermediate circuit after absorbing node k . (c) Updated circuit after combining coupled shunt branches. (d) Circuit after the pseudo inductors conformed by regular inductors.

where

$$M'_{l^\pm,m^\pm} = \frac{1}{\omega^2 \varepsilon_0 S_{l^\pm} S_{m^\pm}} \int_{S_{l^\pm}} \int_{S_{m^\pm}} [G(\mathbf{r}, \mathbf{r}') - G_0(\mathbf{r}, \mathbf{r}')] ds' ds \quad (8)$$

and is depicted by a rectangular bar. In (7), \mathbf{t}_l and \mathbf{t}_m are the unit vectors in the direction of inductive meshes l and m , respectively. w_l and w_m are the width of inductive meshes l and m , respectively. S_{l^\pm} and S_{m^\pm} are the areas of capacitive meshes l^\pm and m^\pm . And μ_0 is permeability in free space.

The G-PEEC model has been proven to be not only physical but also passive [25]. It has been shown that the radiation resistance by a short inductive cell exactly equals to that of a short dipole derived in antenna textbooks.

B. Node-Absorbing Process

The node-absorbing process is a recursive process to redistribute the contributions of the insignificant nodes in the G-PEEC model to the remaining significant nodes. This absorbing process is based on a physically sensible equivalent circuit transformation [24] and a process of combining parallel connected branches under constrains of the broad and narrow sense criteria [25].

To preserve a high fidelity of the nature of the circuit, the transformation introduces temporally a serially connected pseudo inductor to each grounded potior, which will be conformed by the regular inductors at the end of the node-absorbing process. The equivalent circuit transformation that is applied to absorb node k is illustrated in Fig. 2, by which the elements directly connected to node k in Fig. 2(a) are rearranged by incrementally coupled potiors and the coupled inductors as shown in Fig. 2(b). The combining process takes place to

merge all the shunt connected branches one by one, as illustrated by Fig. 2(c). When the node-absorbing process stops, the pseudo inductors will be conflated by regular inductors on the conductor as shown in Fig. 2(d). The combining process takes more than 99% of the computational overhead in the whole MMC derivation, which can be significantly accelerated by GPU parallel computation techniques [26], [27].

Compared with the traditional equivalent circuits of antennas, the MMC exhibits three desirable and unique features: 1) its topology and element values exhibit a clear physical sense of the antenna structure; 2) it retains all the full-wave characteristics including the electric and magnetic couplings among structural segments, the radiation effect, and material losses; and most attractively, 3) it is systematically derived without using intuition.

III. CIRCUITAL FIGURE OF MERIT FOR RADIATION EFFICIENCY

The total antenna efficiency is the product of three efficiencies: the radiation efficiency, the network efficiency that is associated with the loss of the matching/feeding network, and the matching efficiency [28]. The radiation efficiency is defined as “the ratio of the total power radiated by an antenna to the net power accepted by the antenna from the connected transmitter” [29]. This article only concerns with the radiation efficiency, which is an intrinsic property of an antenna structure.

Traditionally, concerning radiation efficiency, only overall radiated power and total antenna losses are focused on. Contribution from the mutual radiation resistance is concealed in the models. Indeed, investigation into the interaction from antenna segments provides a unique perspective to understand the radiation mechanism. It will be shown that it is the mutual radiated power that dominates the radiation efficiency of an antenna.

A. Partially Radiated Power by Antenna Segments

Having had the MMC for an antenna, the partial radiated power can be simply found by finding the consumed power on each partial self- and mutual radiation resistance of antenna segments. According to the Poynting's theorem, the self-radiated power $P_{l,l}^R$ contributed by self-radiation resistance $R_{l,l}^R$ associated with segment l and the current I_l^M flowing through the segment can be expressed as

$$P_{l,l}^R = \frac{1}{2} R_{l,l}^R |I_l^M|^2. \quad (9)$$

Similarly, the mutual radiated power $P_{l,m}^R$ contributed by mutual radiation resistance of segments l and m is

$$P_{l,m}^R = \text{Re}[R_{l,m}^R I_l^M (I_m^M)^*] \quad (10)$$

which involves mutual-radiation resistance $R_{l,m}^R$ and currents I_l^M and I_m^M flowing through segments l and m . The conductor loss consumed by segment l can be found as

$$P_l^C = \frac{1}{2} R_l^C |I_l^M|^2. \quad (11)$$

Equation (9) indicates that self-radiated power of each segment is always positive because the self-radiation resistance is always positive, so is the conductor loss in (11). However, the polarity of mutual radiated power, as stated by (10), depends on the phase difference of the two currents and the sign of $R_{l,m}^R$ that is determined by the relative locations, orientations, and effective sizes of segments l and m . As the total radiated power is the sum of all the partially radiated powers, the positive and negative partially radiated powers contribute to and absorb from the total radiated power, respectively.

B. Circuitual Figure of Merit for Radiation Efficiency

Radiation efficiency η is an important characteristic of an electrically small antenna [4], [7], [28]. To view the nature of antenna radiation from the perspective of the circuit domain, the definition of the radiation efficiency can be written as

$$\eta = \frac{\sum_{l=1}^M \sum_{m=l}^M P_{l,m}^R}{\sum_{l=1}^M P_l^C + \sum_{l=1}^M \sum_{m=l}^M P_{l,m}^R} \quad (12)$$

where M is the number of segments by which the antenna is divided in the MMC.

By separating the self- and mutual radiated power in (12), the definition of the radiation efficiency η can be rewritten as

$$\eta = \frac{\alpha(1 + \beta)}{1 + \alpha(1 + \beta)} \quad (13)$$

where

$$\alpha = \frac{\sum_{l=1}^M P_{l,l}^R}{\sum_{l=1}^M P_l^C} \quad (14)$$

which is the ratio of total partial radiated power contributed by all the self-radiation resistances to total conductor loss, and

$$\beta = \frac{\sum_{l=1}^M \sum_{m=l+1}^M P_{l,m}^R}{\sum_{l=1}^M P_{l,l}^R} \quad (15)$$

which is the ratio of the total partial radiated power of all mutual radiation resistances to that of self-radiation resistances.

Factor α depends on the dimension of the antenna segment rather than antenna overall length. For different antenna segments with the same dimension, the ratio of the self-radiated power to the conductor loss $P_{l,l}^R/P_l^C$ is the same. It can be proved that the factor α is the same as the ratio $P_{l,l}^R/P_l^C$ for each segment in spite of the number of segments.

On the other hand, factor β significantly depends on the configuration of the antenna. For two perpendicular segments, their mutual radiation resistance is zero, so is the mutual radiated power. For two closely placed parallel segments, their mutual radiation resistance is positive. However, their mutual radiated power could be positive if two currents are in phase or negative if the currents are out of phase. Therefore, the factor β will dominate the radiation efficiency, and is an important figure of merit.

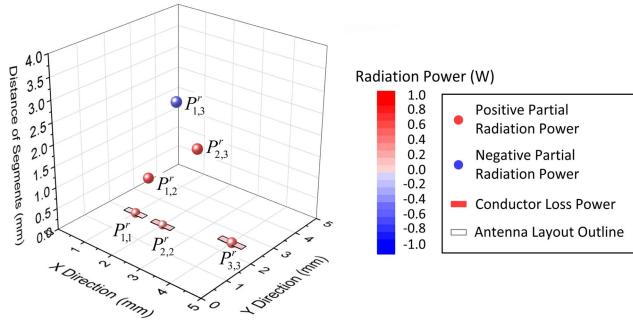


Fig. 3. Holographic radiation diagram of three segments.

C. Holographic Radiation Diagram

To further understand the radiation mechanism of an antenna with respect to a given structure, the holographic radiation diagram for illustrating the correspondence of the partial radiated power and concerned antenna segments is proposed. Fig. 3 shows a simple example of the radiation diagram with three antenna segments, in which the conductor loss and the self-radiated power of a segment are expressed by a rectangle bar and a ball marker with a warm color overlaid with and at the center of the segment layout, respectively. The mutual radiated power of two segments is represented by a colored ball marker located at the point whose (x, y) coordinates are the project of the geometric center point of the centers of the two segments on xy plane and the z coordinate equals to the z coordinate of the geometric center point plus the distance between the centers of the two segments. The warm-colored balls and the cool-colored balls express positive and negative radiated power, respectively. The diameter of a ball and its color grade are proportional to the magnitude of the partial radiated power.

Three useful information can be directly observed from a holographic radiation: 1) the contributions of partial self-radiated power and conductor loss of each segment; 2) the portions of positive and negative partial mutual radiated powers; and 3) the origin of the negative partial radiated power.

D. CMs of MMC

The theory of CMs, as a promising means of antenna design, has regained attention in the community in recent years [20]–[22]. It is interesting to find that CMs can also be found using the concise MMC very efficiently since its model order is usually one order of magnitude smaller than the original G-PEEC model.

The CMs problem can be formulated by eigen decomposition of the resistance matrix \mathbf{R} and reactance matrix \mathbf{X} of an MMC as

$$\mathbf{X}\mathbf{J}_n = \lambda_n \mathbf{R}\mathbf{J}_n \quad (16)$$

where \mathbf{J}_n is the current distribution of the n th CM and λ_n is the ratio of the reactive power $\langle \mathbf{J}_n^*, \mathbf{X}\mathbf{J}_n \rangle$ to the consumed power $\langle \mathbf{J}_n^*, \mathbf{R}\mathbf{J}_n \rangle$, including the radiated energy and energy loss. When $\lambda_n = 0$, the reactive power is zero and the corresponding CM is a resonant mode, which is presumably a working mode for the antenna.

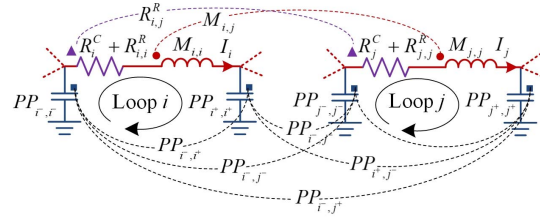


Fig. 4. MMC and respective current loops for CMs eigen equation.

As shown in Fig. 4, each inductor with its two connected pots of an MMC constitutes one loop equation. The resistance matrix \mathbf{R} and reactance matrix \mathbf{X} can be found from these loop equations that are associated with the loop voltages and currents by

$$\mathbf{V} = (\mathbf{R} + j\mathbf{X})\mathbf{I}. \quad (17)$$

For the i th loop, its loop voltage V_i is constituted by all the loop currents in the circuit as

$$\begin{aligned} V_i = & \left[R_i^C + R_{i,i}^R + j\omega M_{i,i} \right. \\ & \left. + \frac{1}{j\omega} (PP_{i-,i-} - 2PP_{i-,i+} + PP_{i+,i+}) \right] I_i \\ & + \sum_{j \neq i} \left[R_{i,j}^R + j\omega M_{i,j} + \frac{1}{j\omega} (PP_{i-,j-} - PP_{i-,j+} \right. \\ & \left. - PP_{i+,j-} + PP_{i+,j+}) \right] I_j. \end{aligned} \quad (18)$$

Therefore, the self-terms $R_{i,i}$, $X_{i,i}$ and the mutual terms $R_{i,j}$, $X_{i,j}$ can be obtained as

$$R_{i,i} = R_i^C + R_{i,i}^R \quad (19)$$

$$R_{i,j} = R_{i,j}^R \quad (20)$$

$$X_{i,i} = \omega M_{i,i} - \frac{1}{\omega} (PP_{i-,i-} - 2PP_{i-,i+} + PP_{i+,i+}) \quad (21)$$

$$X_{i,j} = \omega M_{i,j} - \frac{1}{\omega} (PP_{i-,j-} - PP_{i-,j+} - PP_{i+,j-} + PP_{i+,j+}). \quad (22)$$

For a given frequency, the eigenmodes \mathbf{J}_n and corresponding eigenvalues λ_n of (16) can be found by solving the eigen equation.

IV. ILLUSTRATION EXAMPLES

Having introduced the circuitual figure of merit for radiation efficiency and prepared the analysis tool for CMs using an MMC, the best way to show the accuracy, usefulness, and effectiveness of a full-wave MMC to an antenna problem is to go through practical examples. In this section, three typical antenna configurations are studied, which are a strip dipole antenna, a meander strip dipole antenna, and a loop antenna. It will be shown that the MMC and the introduced circuitual figure of merit not only provide a comprehensive physical insight about the antenna radiation but also reveal the root cause that deteriorates the radiation efficiency.

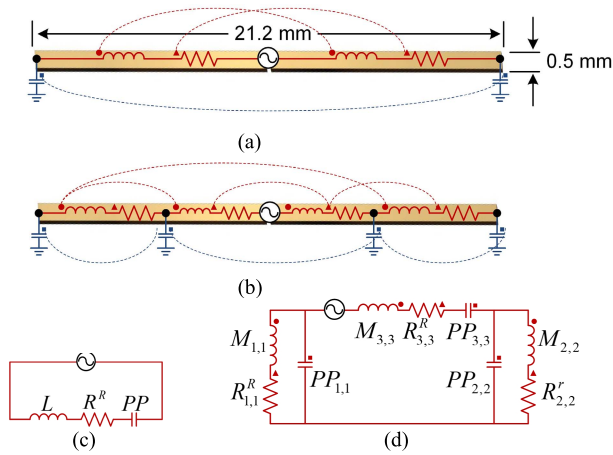


Fig. 5. MMCs of a dipole antenna. (a) Layout and its MMC for the half-wave mode. (b) Layout and its MMC for the full-wave mode. (c) Further simplified circuit for the half-wave mode. (d) Further simplified circuit for the full-wave mode.

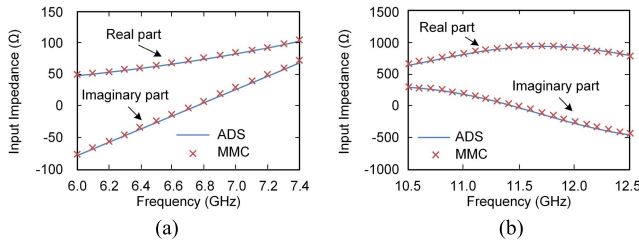


Fig. 6. Input impedance of the dipole antenna simulated by ADS and MMC. (a) Input impedance for the half-wave mode. (b) Input impedance for the full-wave mode.

A. Physical MMC Model for Antennas

This is a “hello world” example to show how the MMC is applied to an antenna. Assume the thin metal strip dipole antenna shown in Fig. 5(a) works in two different modes: the half-wave mode at 6.7 GHz and the full-wave mode at 11.5 GHz. The derived MMCs for the half-wave and the full-wave modes are embedded in the layout of the antenna in Fig. 5(a) and (b), respectively, in which circle dots stand for inductive mutual coupling, square dots represent capacitive coupling, and triangle dots indicate mutual radiation resistance. It is worth mentioning that each inductor represents the aggregated characteristics of a segment of the antenna. In this simple example, a perfect conductor is assumed.

With further simplification as illustrated in Appendix, more concise circuit models for the half-wave and the full-wave dipoles are found to be an RLC series-connected circuit, as shown in Fig. 5(c), and a shunt-connected circuit, as shown in Fig. 5(d), respectively. The comparisons of the input impedances obtained by the MMC models and those by commercial software ADS [30], which is based on the full-wave method of moments, for the half-wave and the full-wave dipoles are shown in Fig. 6(a) and (b), respectively. Excellent agreement further justifies that a half-wave dipole antenna does work in the series resonance mode and a full-wave dipole antenna exhibits a shunt resonance at frequencies of 6.7 and 11.5 GHz, respectively. The element values versus frequency

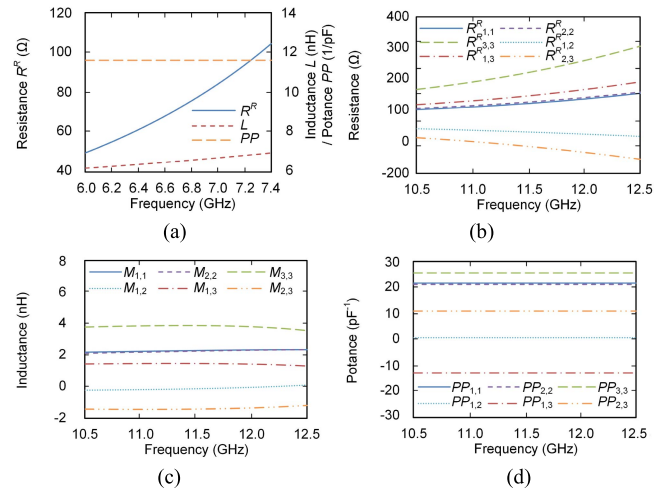


Fig. 7. Element values of the MMC for the dipole antenna. (a) Resistance R^R , inductance L , and potance PP for the half-wave mode. (b) Resistances $R_{1,1}^R$, $R_{2,2}^R$, $R_{3,3}^R$, $R_{1,2}^R$, $R_{1,3}^R$, and $R_{2,3}^R$ for the full-wave mode. (c) Inductances $M_{1,1}$, $M_{2,2}$, $M_{3,3}$, $M_{1,2}$, $M_{1,3}$, and $M_{2,3}$ for the full-wave mode. (d) Potances $PP_{1,1}$, $PP_{2,2}$, $PP_{3,3}$, $PP_{1,2}$, $PP_{1,3}$, and $PP_{2,3}$ for the full-wave mode.

of the MMCs are plotted in Fig. 7, showing that the radiation resistances and inductances vary with the frequency monotonically whereas the potances remain constant as they should be.

B. Antenna Efficiency Explained by MMC Model

To illustrate how the mutual radiated power dominates the radiation efficiency, three typical electrically small antennas with the same largest dimension of 60 mm are investigated. In this study, the conductor thickness and conductivity are chosen to be 0.3 mm and $3.4 \times 10^7 \text{ s} \cdot \text{m}^{-1}$ to account for surface roughness, respectively. The three examinational antennas are a straight thin strip dipole shown in Fig. 8(a), a meander thin strip dipole shown in Fig. 8(b), and a strip loop antenna shown in Fig. 8(c). The most simplified MMCs for both the straight dipole and the meander dipole have the same circuit topology of the RLC serially connected circuits shown in Fig. 9(a) in the frequency range of the first resonant mode. However, their element values are different as compared in Table I. The most simplified MMCs for the loop antenna at 0.2 and 1 GHz are different, and are shown in Fig. 9(b) and (c), respectively. The circuit transformations to obtain Fig. 9(a)–(c) are given in Appendix. The element values listed in Table I illustrate that the circuit for the loop antenna at 0.2 GHz is inductive and that the circuit is dominated by the RLC tanks at 1 GHz, distinguishing different working modes.

MMCs can also be used to easily and accurately calculate the radiation efficiency according to (13). As shown in Fig. 10(a), the calculated radiation efficiencies by MMCs are verified by an in-house full-wave MoM-based EM simulation software. As compared in Table II, the calculated radiation efficiency also very well matches the average measured radiation efficiency at selected frequencies, at which the reflection coefficients are reasonably low for measuring the radiation efficiency without using a matching network. The measured radiation efficiency has excluded the reflection loss from the measured total radiation efficiency with the in-house

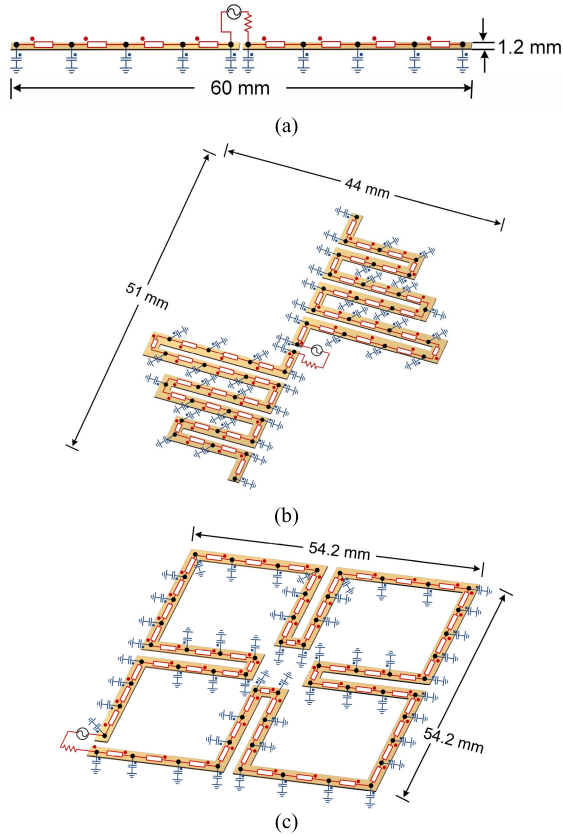


Fig. 8. Layouts and MMCs of three antennas. (a) Straight dipole antenna. (b) Meander dipole antenna. (c) Loop antenna.

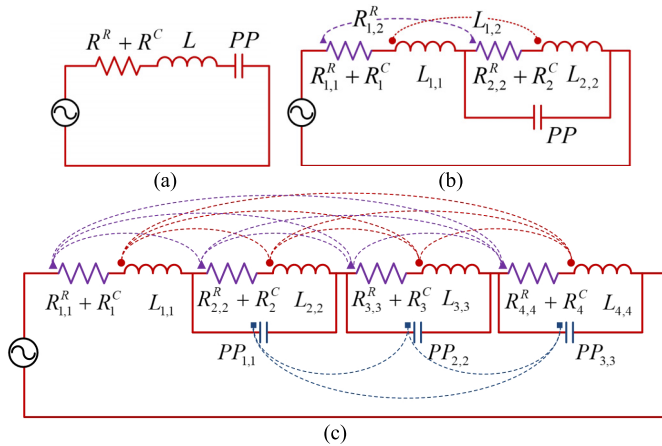


Fig. 9. Most simplified MMCs of three antennas. (a) MMC of the straight dipole antenna and meander dipole antenna at 0.2 and 1 GHz. (b) MMC of the loop antenna at 0.2 GHz. (c) MMC of the loop antenna at 1 GHz.

SATIMO SG-128 spherical near-field scanner [31]. In the measurement, a sleeve balun is used to feed the antennas.

To separately assess the self- and mutual radiated power to the radiation efficiency, the figure of merit, i.e., α and β factors, of the three antennas are compared in Fig. 10(b) and (c). Photographs of the antenna specimens that are made of a copper sheet for efficiency measurement are shown in Fig. 11.

TABLE I
ELEMENT VALUES OF DIPOLE ANTENNA, MEANDER DIPOLE ANTENNA, AND LOOP ANTENNA AT 0.2 AND 1 GHz

Dipole antenna		Meander dipole antenna			
	0.2 GHz	1 GHz			
R^R (Ω)	0.16	4.57	R^R (Ω)	0.22	9.45
R^C (Ω)	0.08	0.19	R^C (Ω)	0.29	1.40
L (nH)	12.12	12.81	L (nH)	32.41	45.05
PP (pF^{-1})	3.67	3.67	PP (pF^{-1})	2.07	2.07
Loop antenna					
	0.2 GHz	1 GHz		0.2 GHz	1 GHz
$R_{1,1}^R$ (Ω)	0.08	31.77	$R_{3,3}^C$ (Ω)	N/A	60.55
$R_{2,2}^R$ (Ω)	0.13	76.55	$R_{4,4}^C$ (Ω)	N/A	38.27
$R_{3,3}^R$ (Ω)	N/A	765.00	$L_{1,1}$ (nH)	92.29	41.49
$R_{4,4}^R$ (Ω)	N/A	496.44	$L_{2,2}$ (nH)	75.61	85.21
$R_{1,2}^R$ (Ω)	0.08	41.67	$L_{3,3}$ (nH)	N/A	41.58
$R_{2,3}^R$ (Ω)	N/A	223.14	$L_{4,4}$ (nH)	N/A	26.83
$R_{2,4}^R$ (Ω)	N/A	163.95	$PP_{1,1}$ (pF^{-1})	1.22	2.78
$R_{3,4}^R$ (Ω)	N/A	596.74	$PP_{2,2}$ (pF^{-1})	N/A	1.50
$R_{1,1}^C$ (Ω)	0.62	3.18	$PP_{3,3}$ (pF^{-1})	N/A	2.03
$R_{2,2}^C$ (Ω)	0.50	8.48			

TABLE II
ANTENNA EFFICIENCIES OBTAINED BY MMC AND MEASUREMENT

Antenna	Frequency (GHz)	Measured Reflection Coefficient (dB)	Simulated Efficiency % (Average)	Measured Efficiency % (Average)
Loop	1.04 ~ 1.08	-27.3 ~ -7.47	96	94
Meander Dipole	1.08 ~ 1.13	-6.11 ~ -5.31	88	89
Dipole	2.44 ~ 2.52	-15.5 ~ -14.5	99	94

It can be observed from Fig. 10(a) that even though the maximum dimensions of the three antennas are the same, their radiation efficiencies differ greatly, among which the radiation efficiency of the straight dipole that is with the shortest length of metal strip is obviously the highest. The efficiency of the loop antenna is next to zero at low frequencies but becomes comparable to that of the straight dipole in the frequency range of 0.6–1.6 GHz. It is noted that the efficiency drops significantly at 1.8 GHz. The mechanism for the drop will be comprehensively studied in Section V.

To investigate the root cause of the difference, the MMCs with a reasonable number of segments are created and are overlaid on the corresponding antenna layout in Fig. 8, in which the nodes of the circuit models are located at their respective physical positions. As can be seen, each MMC consists of some composite inductances that are marked by rectangular boxes and real-valued capacitances to the ground that refers to the zero-potential reference at infinity. Each composite inductance comprises a self-radiation resistance, a conductor loss resistance, and a real inductance all in series, in conjunction with all the relevant mutual couplings. The circular dot next to a composite inductance represents the mutual radiation resistance and the real mutual inductance with other composite inductances. For a fair comparison, the dimensions of all the antenna segments in the three MMCs

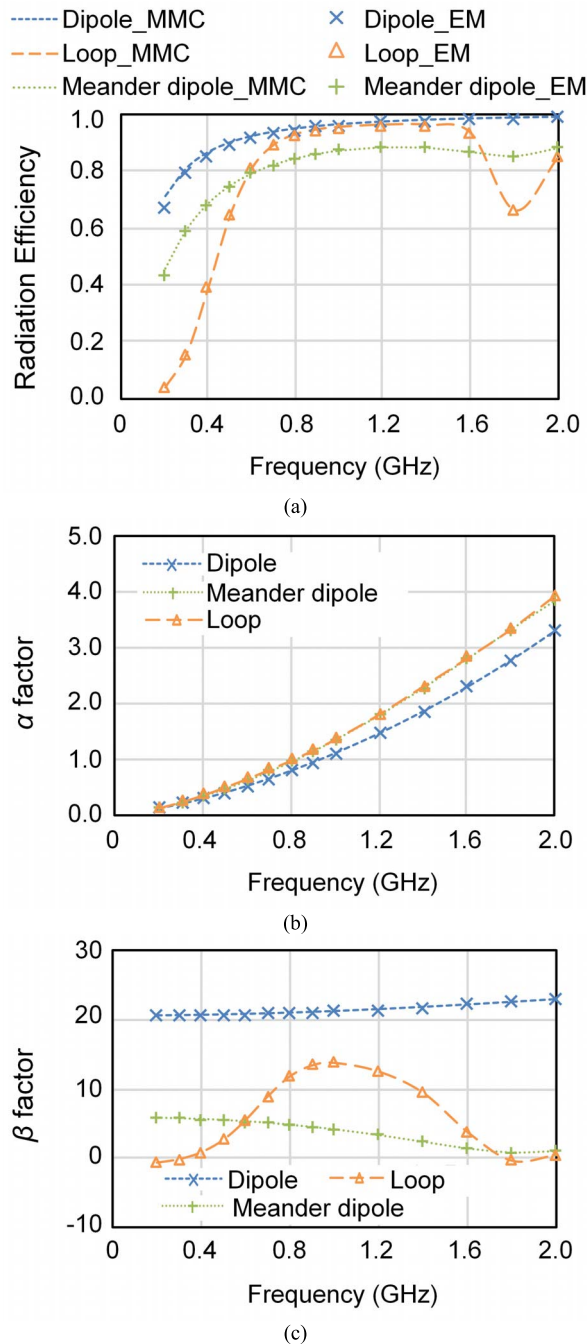


Fig. 10. Radiation characteristics of the three examinational antennas. (a) Radiation efficiency calculated by MMCs and EM model. (b) α factors calculated by MMCs. (c) β factors calculated by MMCs.

are comparable to a short conductor strip of the same width with the length of 7.5 mm.

As presented in Fig. 10(b) and (c), the α factors of the three antennas are close to each other, stating that the radiation efficiency is not dominated by the total self-radiated power as well as the total length of the antenna; the β factors of the three antennas differ from each other significantly, particularly, the β factor of the straight dipole is much larger than those of other two antennas in the whole frequency band, and so is its radiation efficiency. The β factor of the

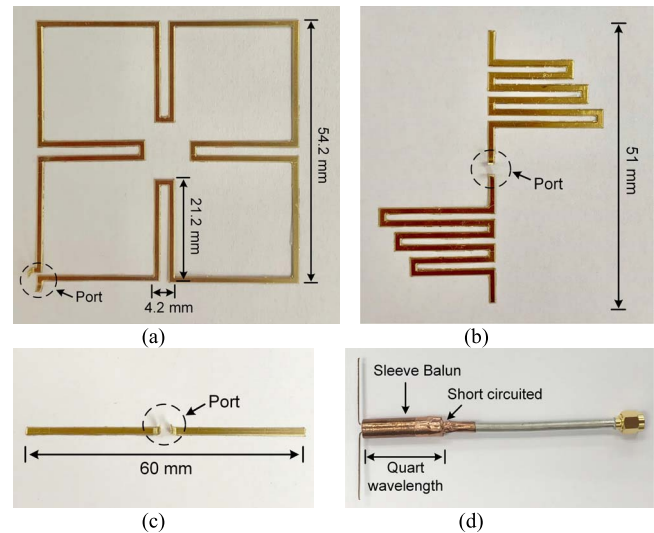


Fig. 11. Photographs of the antenna specimens for efficiency measurement. (a) Loop antenna. (b) Meander dipole antenna. (c) Dipole antenna. (d) Sleeve balun used for feeding the antennas.

meander dipole antenna is small, and therefore its radiation efficiency is low. In the extreme case, the β factor of the loop antenna at low frequencies becomes negative due to that the negative mutual radiated power is more than the positive mutual radiated power. As a result, the self-radiated power is neutralized, leading to a very low total radiation efficiency. With the increase of frequency, the β factor of the loop antenna increases significantly in the frequency band of 0.6–1.6 GHz, and so does the radiation efficiency. The β factor of the loop antenna drops significantly at 1.8 GHz, so does its radiation efficiency. These facts demonstrate that the radiation efficiency is mainly determined by the mutual radiated power and that a critical task to improve the radiation efficiency is to maximize the β factor.

The holographic radiation diagrams of the three antennas at 0.2 and 1 GHz with the same input power can further justify the aforementioned statement. As shown in Fig. 12, the change of the radiated power and conductor loss can explain the observation on the β factor. The holographic diagrams show that the power dissipated on conductor decreases and the self-radiated power increases significantly as the frequency is increased from 0.2 to 1 GHz due to the significant increase of the self-radiation resistances as compared to the surface resistance of a conductor, resulting in the increased α factor.

By comparing the holographic radiation diagrams of the three antennas shown in Fig. 12(a)–(h), it is apparently seen that the straight dipole antenna only generates positive mutual radiated power and that the total mutual radiated power is much larger than that of self-radiated power. This observation explains why the straight dipole exhibits the highest β factor among the three antennas in the frequency band. For the meander dipole antenna, its negative and positive mutual radiated power is comparable, and thus its β factor approaches zero at high frequencies. For the loop antenna, the total negative mutual radiated power is far smaller than the total

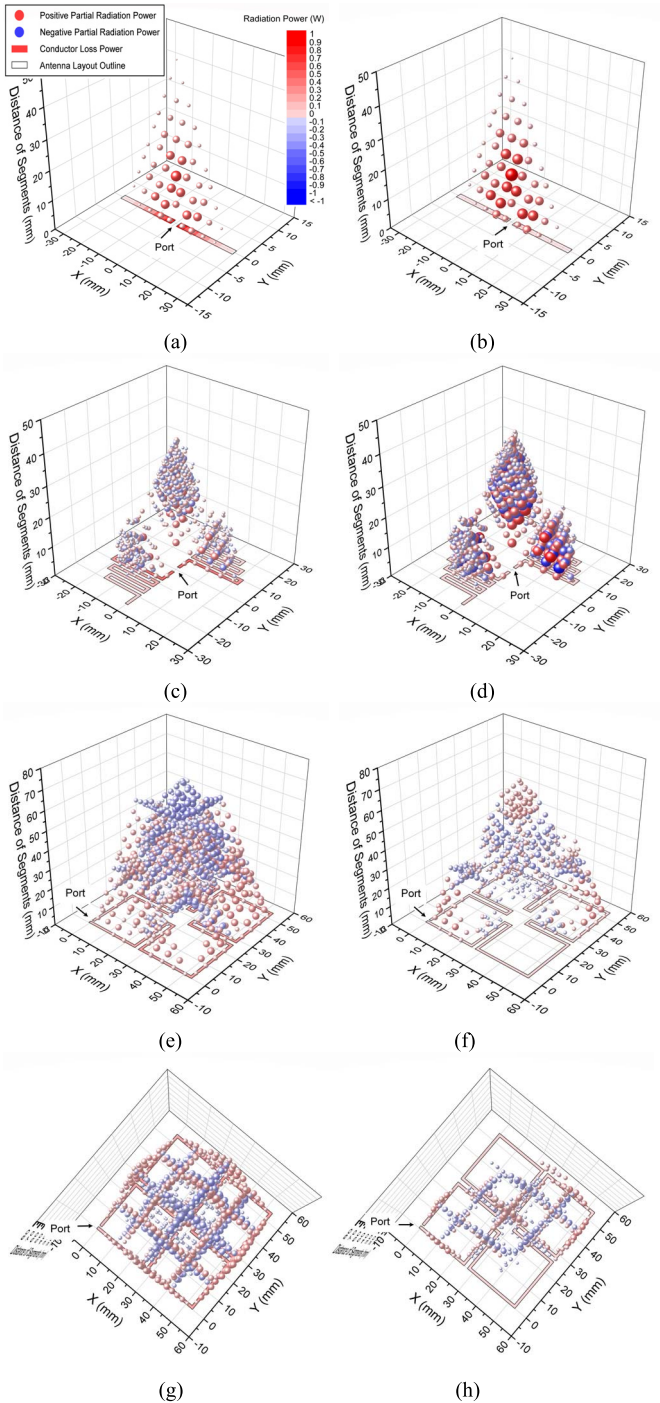


Fig. 12. Holographic radiation diagrams for (a) straight dipole antenna at 0.2 GHz, (b) straight dipole antenna at 1 GHz, (c) meander dipole antenna at 0.2 GHz, (d) meander dipole antenna at 1 GHz, (e) loop antenna at 0.2 GHz, (f) loop antenna at 1 GHz, (g) top view of the loop antenna at 0.2 GHz, and (h) top view of the loop antenna at 1 GHz.

positive mutual radiated power. As a result, its β factor is smaller than that of the straight dipole antenna but is much larger than that of the meander dipole antenna. As shown in Fig. 12(e) or (g), and Fig. 12(f) or (h), there are two working modes for the loop antenna at 0.2 and 1.0 GHz with different current distributions and mutual radiation resistances at the two frequencies.

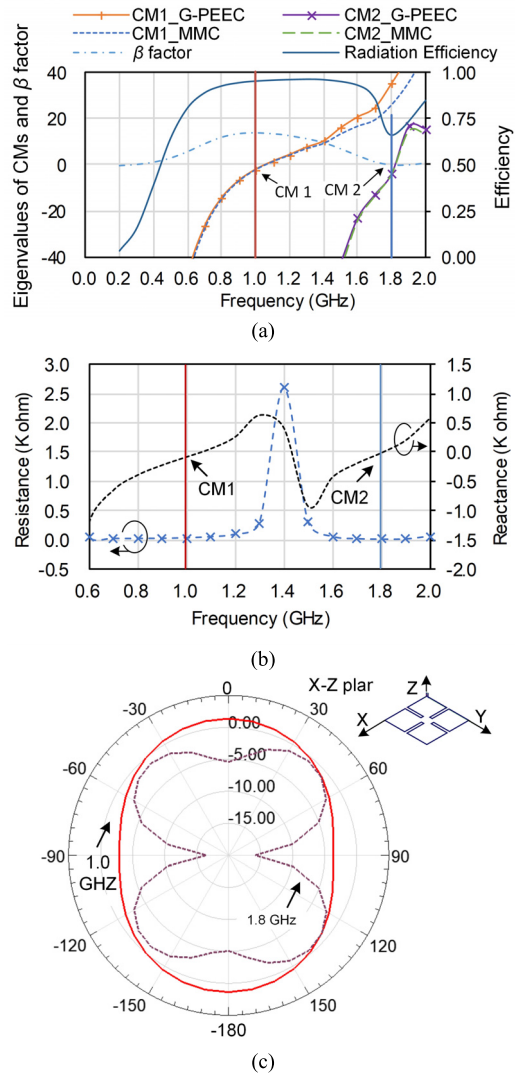


Fig. 13. Radiation efficiency, input impedance, and gain of the loop antenna. (a) Radiation efficiency, β factor, CMs calculated by G-PEEC, and MMC of the loop antenna. (b) Input impedance of the loop antenna calculated by G-PEEC. (c) Gain (in dBi) of the loop antenna at 1.0 and 1.8 GHz in the xz plane calculated by HFSS.

In summary, the antenna radiation efficiency mainly depends on the total positive and negative radiated power, or the β factor, which is in turn determined by the antenna structure and the current distribution at the working frequency. It is worth mentioning that the β factor is irrelevant to the conductor loss. Simply setting the conductor loss to zero in the EM field solver, which equivalently sets the α factor to infinity, could not reveal the fact that the β factor decisively determines the radiation efficiency. To improve the radiation efficiency of an antenna design by revising the antenna structure, it is advisory to look into the holographic radiation diagram and to minimize the total negative mutual radiated power. Section V will demonstrate such an example.

V. APPLICATIONS OF MMC FOR ANTENNA DESIGN

The CMs of an antenna in a frequency range can be calculated efficiently by the MMC. Then the β factor and the holographic radiation diagram of each CM can be used

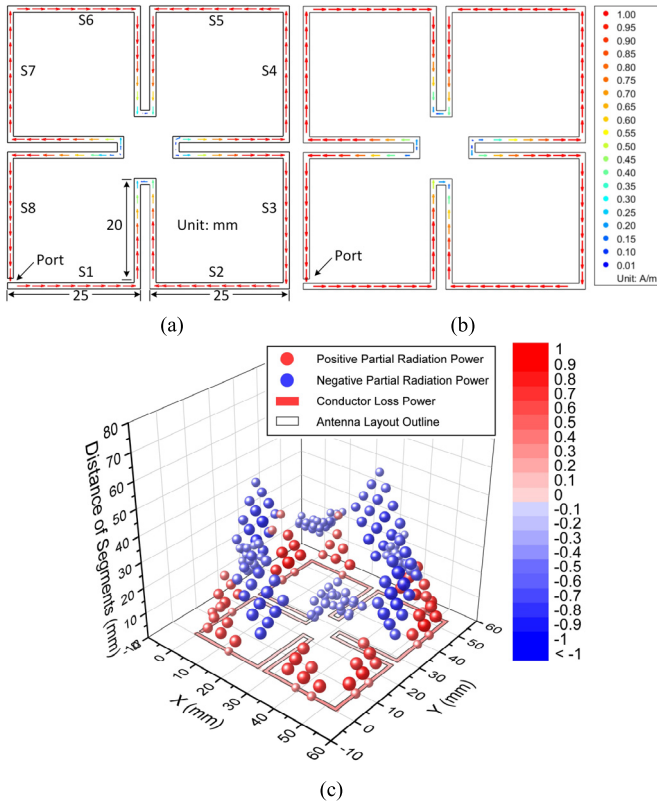


Fig. 14. Current distribution and holographic radiation diagram of design I of the loop antenna at 1.8 GHz. (a) Current distribution with port excited. (b) Current distribution of the CM with port short-circuited. (c) Holographic radiation diagram of the excited current distribution.

to diagnose the usefulness of each CM as well as the “ghost” modes. The ghost modes are referred to those whose β factors are abnormally low as compared to the useful modes.

Referring to the loop antenna in Fig. 8(c), whose calculated radiation efficiency drops drastically around 1.8 GHz and the β factor is negative, as shown in Fig. 10(a) and (c), respectively. To investigate the root cause, the CMs of the loop antenna are obtained by the MMC in the frequency band of interest by short-circuiting the port. The CMs are further verified by those obtained by the G-PEEC. As shown in Fig. 13(a), there are two resonant modes for the loop antenna: CM 1 at 1 GHz and CM 2 at 1.8 GHz. For convenience, the calculated radiation efficiency and the β factor are also superimposed in Fig. 13(a). Fig. 13(b) can indicate the nature of serial resonance of the two modes but cannot explain the difference of their radiation efficiencies. The gains (in dBi) of the loop antenna at 1.0 and 1.8 GHz are calculated by HFSS [32] and are shown in Fig. 13(c). Obviously, the gain at 1.8 GHz, which corresponds to CM 2, is much smaller than that at 1.0 GHz, which works at CM 1, verifying the difference in radiation efficiency. It is seen that not every resonant mode is usable. CM 1 is with the maximum β factor at 1 GHz and therefore is a usable mode, whereas CM 2 at 1.8 GHz corresponds to a negative β factor and is a “ghost” mode, which contributes to the significant drop in the radiation efficiency. The “ghost” CM modes must be avoided in the antenna design.

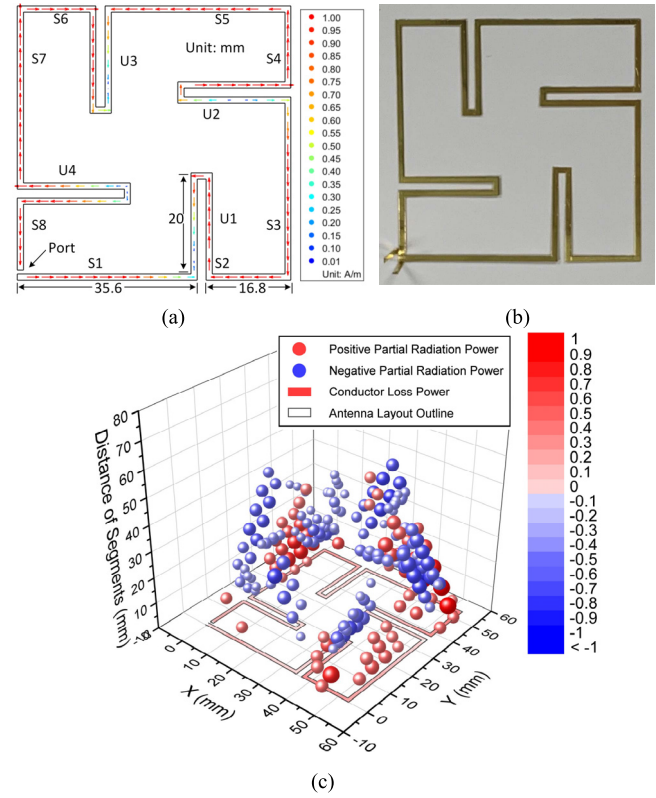


Fig. 15. Current distribution and holographic radiation diagram of design II of the loop antenna at 1.8 GHz. (a) Current distribution. (b) Antenna specimen of design 2 for efficiency measurement. (c) Holographic radiation diagram of the current distribution.

If the loop antenna configuration shown in Fig. 8(c) is named as design 1, its negative β factor at 1.8 GHz suggests that the antenna configuration needs to be revised. To achieve a higher β factor, the current distribution of design 1 at 1.8 GHz is plotted in Fig. 14(a), which is the same as that of the “ghost” CM mode shown in Fig. 14(b). The holographic radiation diagram of the excited current shown in Fig. 14(c) indicates that the negative mutual radiated power is mainly contributed by the pairs of segments on the two symmetric sections of the same side, such as sections S1 and S2 or S3 and S4 shown in Fig. 14(a). Such symmetry needs to be destroyed in order to improve the radiation efficiency.

The first revision of the loop antenna, called design 2, is shown in Fig. 15(a). The antenna specimen for efficiency measurement is made and is shown in Fig. 15(b). The β factor of design 2 is improved from -0.41 of design 1 to 0.50 while the α factor remains 3.3 . The calculated radiation efficiency of design 2 is increased from 66% of design 1 to 83% . The measured radiation efficiency is improved from 57% to 75% , verifying the theoretic value. The current distribution and the holographic radiation diagram of design 2 are shown in Fig. 15(a) and (c), respectively. It can be observed that the negative mutual radiated power between the two sections S1 and S2 is obviously reduced and that the dominant negative radiated power is generated by the mutual coupling within the four reentrant U-shaped sections.

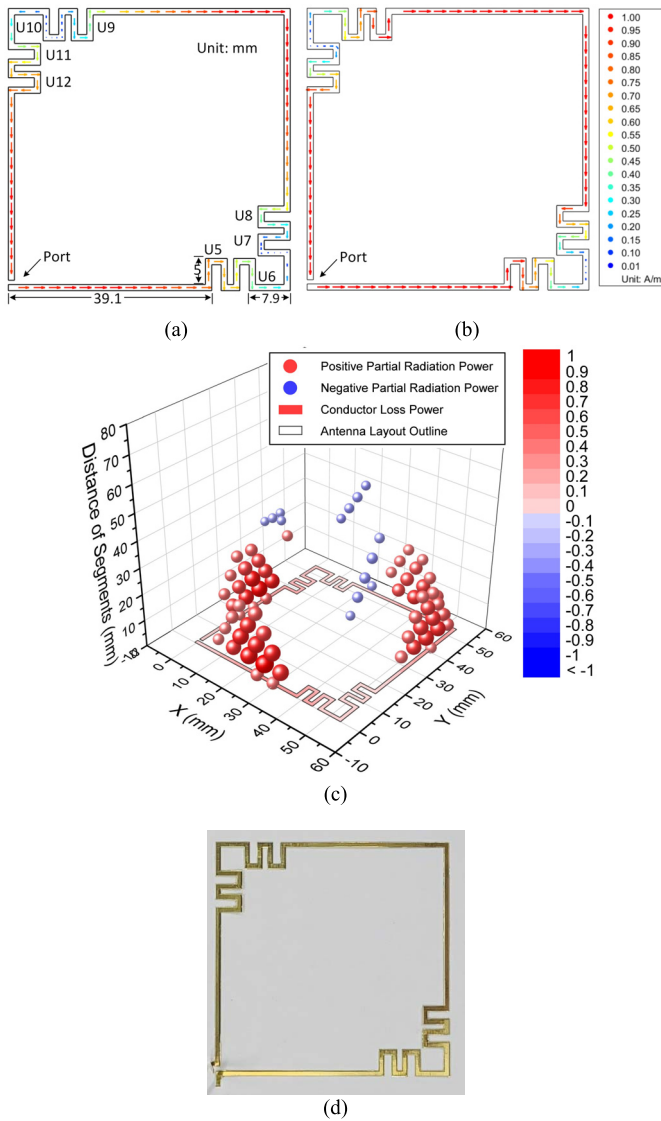


Fig. 16. Current distribution and holographic radiation diagram of design 3 at 1.8 GHz. (a) Current distribution with port excited. (b) Current distribution of the CM with port short-circuited. (c) Holographic radiation diagram of the excited current distribution. (d) Antenna specimen of design 3 for efficiency measurement.

The design is further improved by replacing each long U section [such as U3 in Fig. 15(a)] by two short U sections [such as U9 and U10 in Fig. 16(a)] and arranging the antenna structure symmetrically with respect to the feeding port. The second round redesign is called design 3. The current distribution of design 3 with the port excited by a voltage source is plotted in Fig. 16(a), which is nearly the same as that of the corresponding CM shown in Fig. 16(b). As is demonstrated by the holographic radiation diagram shown in Fig. 16(c), the negative mutual radiated power is almost eliminated. The β factor of design 3 is increased from 0.50 of design 2 to 25, and the α factor remains at 3.3. Consequently, the calculated radiation efficiency of design 3 is improved from 83% of design 2 to 99%. The antenna specimen of design 3 for efficiency measurement is made and is shown in Fig. 16(d). The measured radiation efficiency is as high as 91%, demonstrating that the “ghost” CM is completely

TABLE III
 α FACTOR, β FACTOR, SIMULATED EFFICIENCY, AND MEASURED EFFICIENCY OF THE LOOP ANTENNA FOR THREE DESIGNS AT 1.8 GHz

Antenna	Design 1	Design 2	Design 3
α factor	3.3	3.3	3.3
β factor	-0.41	0.50	25
Calculated Efficiency	66%	83%	99%
Measured Efficiency	57%	75%	91%

eliminated. The measured radiation efficiencies of the original (design 1), the first revision (design 2), and the final revision (design 3) of the loop antenna at 1.8 GHz are compared in Table III. Since a matching circuit is used for measuring the radiation efficiency for each of designs, the measured radiation efficiencies are slightly lower than the theoretical values.

VI. CONCLUSION

In this article, the radiation mechanism of antennas is revealed for the first time from the physical MMC model perspective. It is demonstrated that the MMC model is a general, comprehensive, and physical insightful circuit model for antenna problems. By introducing the β factor, a new circuital figure of merit for radiation efficiency, it is found that the antenna radiation efficiency decisively depends on the total positive and negative mutual radiated power, which are in turn determined by the mutual radiation resistance and the current distribution on the antenna structure at the working frequency. With the aid of the holographic radiation diagram, the origin of negative mutual radiated power can be located, which provides a clear guideline for remedying the antenna design. The holographic radiation diagram can also be used to identify the “ghost” CM.

The proposed new circuital figure of merit has been validated through investigating three typical antennas, theoretically and experimentally. An application of the proposed theory to the antenna design is also demonstrated via designing a highly efficient loop antenna. The physical circuit model can provide multiple aspects of uses for EM radiation-related problems, including designing high-efficiency antennas, identifying unwanted radiation modes of an electronic system, and explaining new EM meta-structures.

APPENDIX

The derived MMCs can be further simplified to study the resonant mode of an antenna. Three types of common MMC topologies can be further simplified.

- 1) Serially connected elements of the same type between two terminals of the source, such as the circuit topology in Fig. 5(a), can be combined as one element according to ohm’s law. The process and updating formulas are given in Fig. 17(a).
- 2) One inductor can be in serially connected with an insignificant potior and in shunt with a significant potior, such as the circuit topology in Fig. 5(b). To express the dominant resonance mode, the insignificant capacitance is absorbed by the significant capacitance with the process given in Fig. 17(b).

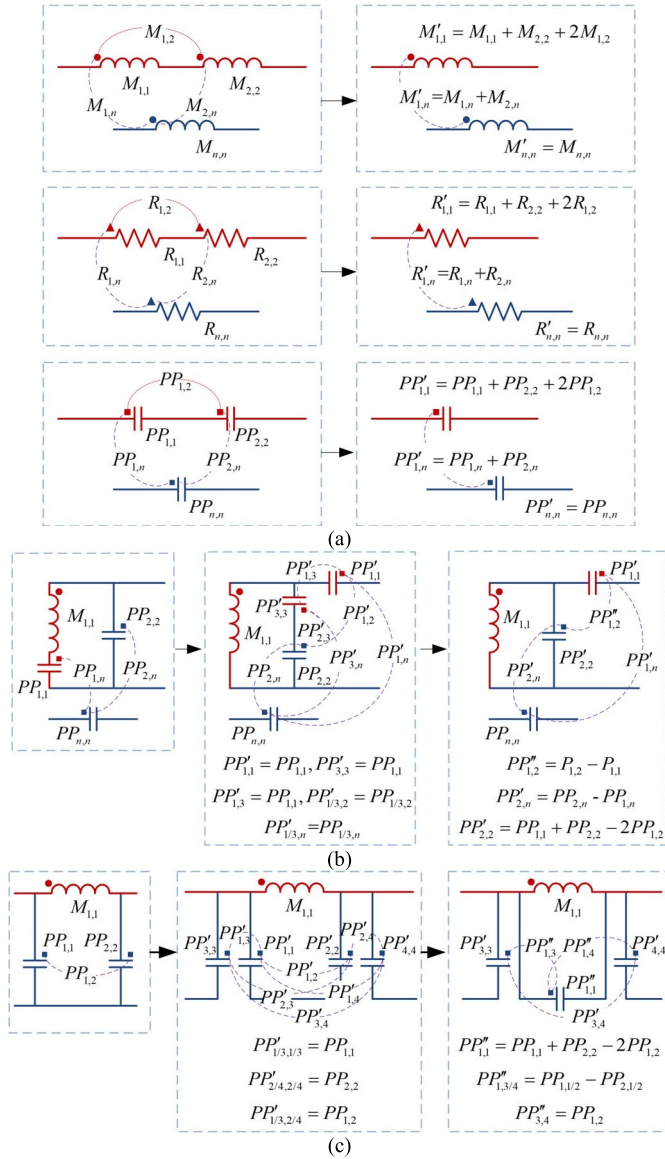


Fig. 17. Process of circuit simplification. (a) Combining two serially connected elements. (b) Extraction of one insignificant potior. (c) Transformation of a Π -network to a tank network.

3) The Π -network that consists of one inductor and two capacitors can be simplified to a tank network with one inductor and one potior as illustrated in Fig. 17(c).

ACKNOWLEDGMENT

The authors sincerely appreciate the valuable comments and constructive suggestions from all the reviewers, an Associate Editor, and the Editor-in-Chief, which make the work much more presentable.

REFERENCES

[1] Wikipedia. *Guglielmo Marconi*. Accessed: Jan. 2019. [Online]. Available: https://en.wikipedia.org/wiki/Guglielmo_Marconi

[2] S. Ramo and J. R. Whinnery, "Circuit concepts and their validity at high frequency," in *Fields and Waves in Modern Radio*. Hoboken, NJ, USA: Wiley, 1944, pp. 175–185.

[3] L. J. Chu, "Physical limitations of omni-directional antennas," *J. Appl. Phys.*, vol. 19, no. 12, pp. 1163–1175, Dec. 1948.

[4] R. F. Harrington, "Effect of antenna size on gain, bandwidth, and efficiency," *J. Res. Nat. Bureau Standards*, vol. 64D, no. 1, pp. 1–12, Jan./Feb. 1960.

[5] V. Losenicky, L. Jelinek, M. Capek, and M. Gustafsson, "Dissipation factors of spherical current modes on multiple spherical layers," *IEEE Trans. Antennas Propag.*, vol. 66, no. 9, pp. 4948–4952, Sep. 2018.

[6] C. Pfeiffer, "Fundamental efficiency limits for small metallic antennas," *IEEE Trans. Antennas Propag.*, vol. 65, no. 4, pp. 1642–1650, Apr. 2017.

[7] H. L. Thal, "Radiation efficiency limits for elementary antenna shapes," *IEEE Trans. Antennas Propag.*, vol. 66, no. 5, pp. 2179–2187, May 2018.

[8] L. Jelinek and M. Capek, "Optimal currents on arbitrarily shaped surfaces," *IEEE Trans. Antennas Propag.*, vol. 65, no. 1, pp. 329–341, Jan. 2017.

[9] C. Cho, J.-S. Kang, and H. Choo, "Improved wheeler cap method based on an equivalent high-order circuit model," *IEEE Trans. Antennas Propag.*, vol. 62, no. 1, pp. 274–281, Jan. 2014.

[10] J. Holopainen, R. Valkonen, O. Kivekas, J. Ilvonen, and P. Vainikainen, "Broadband equivalent circuit model for capacitive coupling element-based mobile terminal antenna," *IEEE Antennas Wireless Propag. Lett.*, vol. 9, pp. 716–719, 2010.

[11] M. I. Sobhy, B. Sanz-Izquierdo, and J. C. Batchelor, "System and circuit models for microwave antennas," *IEEE Trans. Microw. Theory Techn.*, vol. 55, no. 4, pp. 729–735, Apr. 2007.

[12] D.-R. Shin, G. Lee, and W. S. Park, "Simplified vector potential and circuit equivalent model for a normal-mode helical antenna," *IEEE Antennas Wireless Propag. Lett.*, vol. 12, pp. 1037–1040, 2013.

[13] K. Carver and J. Mink, "Microstrip antenna technology," *IEEE Trans. Antennas Propag.*, vol. 29, no. 1, pp. 323–326, Jan. 1981.

[14] T. G. Tang, Q. M. Tieng, and M. W. Gunn, "Equivalent circuit of a dipole antenna using frequency-independent lumped elements," *IEEE Trans. Antennas Propag.*, vol. 41, no. 1, pp. 100–103, Jan. 1993.

[15] O. O. Olaode, W. D. Palmer, and W. T. Joines, "Effects of meandering on dipole antenna resonant frequency," *IEEE Antennas Wireless Propag. Lett.*, vol. 11, pp. 122–125, Jan. 2012.

[16] A. E. Ruehli, "Equivalent circuit models for three-dimensional multi-conductor systems," *IEEE Trans. Microw. Theory Techn.*, vol. 22, no. 3, pp. 216–221, Mar. 1974.

[17] L. K. Yeung and K.-L. Wu, "Generalized partial element equivalent circuit (PEEC) modeling with radiation effect," *IEEE Trans. Microw. Theory Techn.*, vol. 59, no. 10, pp. 2377–2384, Oct. 2011.

[18] Y. S. Cao, L. J. Jiang, and A. E. Ruehli, "Distributive radiation and transfer characterization based on the PEEC method," *IEEE Trans. Electromagn. Compat.*, vol. 57, no. 4, pp. 734–742, Aug. 2015.

[19] C.-C. Chou, W.-C. Lee, and T.-L. Wu, "A rigorous proof on the radiation resistance in generalized PEEC model," *IEEE Trans. Microw. Theory Techn.*, vol. 64, no. 12, pp. 4091–4097, Dec. 2016.

[20] R. F. Harrington and J. R. Mautz, "Theory of characteristic modes for conducting bodies," *IEEE Trans. Antenna Propag.*, vol. 19, no. 5, pp. 622–628, Sep. 1971.

[21] R. F. Harrington, J. R. Mautz, and Y. Chang, "Characteristic modes for dielectric and magnetic bodies," *IEEE Trans. Antenna Propag.*, vol. 20, no. 2, pp. 194–198, Mar. 1972.

[22] Y. Chen and C. F. Wang, *Characteristic Modes: Theory and Applications in Antenna Engineering*. Hoboken, NJ, USA: Wiley, 2015.

[23] M. Capek, J. Eichler, and P. Hazdra, "Evaluating radiation efficiency from characteristic currents," *IET Microw., Antennas Propag.*, vol. 9, no. 1, pp. 10–15, Jan. 2015.

[24] Y. Dou and K.-L. Wu, "A passive PEEC-based micromodeling circuit for high-speed interconnection problems," *IEEE Trans. Microw. Theory Techn.*, vol. 66, no. 3, pp. 1201–1214, Mar. 2018.

[25] Y. Dou and K.-L. Wu, "A passive full-wave micromodeling circuit for packaging and interconnection problems," *IEEE Trans. Microw. Theory Techn.*, vol. 67, no. 6, pp. 2197–2207, Jun. 2019.

[26] Y. Dou and K.-L. Wu, "Acceleration of parallel computation for derived micro-modeling circuit by exploiting GPU memory bandwidth limit," in *Proc. IEEE MTT-S Int. Conf. Numer. Electromagn. Multiphys. Modeling Optim. RF, Microw., Terahertz Appl. (NEMO)*, Seville, Spain, May 2017, pp. 146–148.

[27] Y. Dou and K.-L. Wu, "Acceleration of a physically derived micro-modeling circuit for packaging problems using graphics processing units," in *IEEE MTT-S Int. Microw. Symp. Dig.*, Honolulu, HI, USA, Jun. 2017, pp. 1638–1640.

- [28] M. Shahpari and D. V. Thiel, "Fundamental limitations for antenna radiation efficiency," *IEEE Trans. Antennas Propag.*, vol. 66, no. 8, pp. 3894–3901, Aug. 2018.
- [29] *IEEE Standard for Definitions of Terms for Antennas*, IEEE Standard 145-2013, Mar. 2014, pp. 1–50.
- [30] *Momentum RF, Momentum*, Keysight EEsof, Inc. Santa Clara, CA, USA, 2017.
- [31] *Multi-Probe Systems SG 128*. Accessed: Oct. 2019. [Online]. Available: <https://www.mvg-world.com/products/antenna-measurement/multi-probe-systems/sg-128>
- [32] *HFSS*, Ansys, Inc., Canonsburg, PA, USA, 2019.



Yuhang Dou (Member, IEEE) received the B.S. degree from the Nanjing University of Science and Technology, Nanjing, China, in 2012, and the Ph.D. degree from The Chinese University of Hong Kong, Hong Kong, in 2019.

She is currently a Post-Doctoral Fellow with the School of Engineering and Computer, Purdue University, West Lafayette, IN, USA. Her current research interests include fast signal integrity (SI) analysis of large-scale linear/nonlinear circuits and systems, and physics-based circuit-domain modeling

methods for radiation and high-speed microwave problems.

Dr. Dou was a recipient of first runner up awards in both 2015 and 2018 IEEE Hong Kong AP/MTT Postgraduate Conference. She also won the Honorable Mention Award in 2015 IEEE MTT-S International Conference on Numerical Electromagnetic and Multiphysics Modeling and Optimization for RF, Microwave, and Terahertz Applications (NEMO).



Ke-Li Wu (Fellow, IEEE) received the B.S. and M.Eng. degrees from the Nanjing University of Science and Technology, Nanjing, China, in 1982 and 1985, respectively, and the Ph.D. degree from Laval University, Quebec, QC, Canada, in 1989.

From 1989 to 1993, he was a Research Engineer with McMaster University, Hamilton, ON, Canada. He joined COM DEV (now Honeywell Aerospace), Cambridge, ON, in 1993, where he was a Principal Member of Technical Staff. Since 1999, he has been with The Chinese University of Hong Kong,

Hong Kong, where he is currently a Professor and the Director of the Radiofrequency Radiation Research Laboratory. His current research interests include EM-based circuit domain modeling of high-speed interconnections, robot automatic tuning of microwave filters, decoupling techniques of MIMO antennas, and Internet of Things (IoT) technologies.

Prof. Wu is a member of the IEEE MTT-8 Subcommittee. He was a recipient of the 1998 COM DEV Achievement Award and the Asia-Pacific Microwave Conference Prize twice in 2008 and 2012, respectively. He was an Associate Editor of the IEEE TRANSACTIONS ON MICROWAVE THEORY AND TECHNIQUES (MTT) from 2006 to 2009.